Intracellular Delivery of Poorly Soluble Polyphenols: Elucidating the Interplay of Self-Assembling Nanocarriers and Human Chondrocytes

Birthe Kann,[†,‡] Christian Spengler,[§] Karine Coradini,[∥] Lucas A. Rigo,[∥] Martin L. Bennink,[⊥] Karin Jacobs,[§] Herman L. Offerhaus,[‡] Ruy C. R. Beck,[∥] and Maike Windbergs[*,†,#,∇]

[†]Saarland University, Department of Biopharmaceutics and Pharmaceutical Technology, Campus A4.1, 66123 Saarbruecken, Germany

[‡]University of Twente, Optical Sciences Group, MESA+ Institute for Nanotechnology, P.O. Box 217, 7500 AE Enschede, The Netherlands

[§]Saarland University, Experimental Physics, Campus E2.9, 66123 Saarbruecken, Germany

[∥]Programa de Pós-Graduação em Ciências Farmacêuticas, Faculdade de Farmácia, Federal University of Rio Grande do Sul (UFRGS), 90610-000, Porto Alegre, Rio Grande do Sul, Brazil

[⊥]University of Twente, Nanobiophysics Group, MESA+ Institute for Nanotechnology, P.O. Box 217, 7500 AE Enschede, The Netherlands

[#]Helmholtz Centre for Infection Research and Helmholtz Institute for Pharmaceutical Research Saarland, Department of Drug Delivery, Campus E 8.1, 66123 Saarbruecken, Germany

[∇]PharmBioTec GmbH, Department of Drug Delivery, Science Park 1, 66123 Saarbruecken, Germany

ABSTRACT: Increased molecular understanding of multifactorial diseases paves the way for novel therapeutic approaches requiring sophisticated carriers for intracellular delivery of actives. We designed and characterized self-assembling lipid-core nanocapsules for coencapsulation of two poorly soluble natural polyphenols curcumin and resveratrol. The polyphenols were identified as high-potential therapeutic candidates intervening in the intracellular inflammation cascade of chondrocytes during the progress of osteoarthritis. To elucidate the interplay between chondrocytes and nanocapsules and their therapeutic effect, we pursued a complementary analytical approach combining label-free visualization with biological assays. Primary human chondrocytes did not show any adverse effects upon nanocapsule application and coherent anti-Stokes Raman scattering images visualized their intracellular uptake. Further, by systematically blocking different uptake mechanisms, an energy independent uptake into the cells could be identified. Additionally, we tested the therapeutic effect of the polyphenol-loaded carriers on inflamed chondrocytes. Treatment with nanocapsules resulted in a major reduction of nitric oxide levels, a well-known apoptosis trigger during the course of osteoarthritis. For a more profound examination of this protective effect on joint cells, we pursued studies with atomic force microscopy investigations. Significant changes in the cell cytoskeleton as well as prominent dents in the cell membrane upon induced apoptosis were revealed. Interestingly, these effects could not be detected for chondrocytes which were pretreated with the nanocapsules. Overall, besides presenting a sophisticated carrier system for joint application, these results highlight the necessity of establishing combinatorial analytical approaches to elucidate cellular uptake, the interplay of codelivered drugs and their therapeutic effect on the subcellular level.
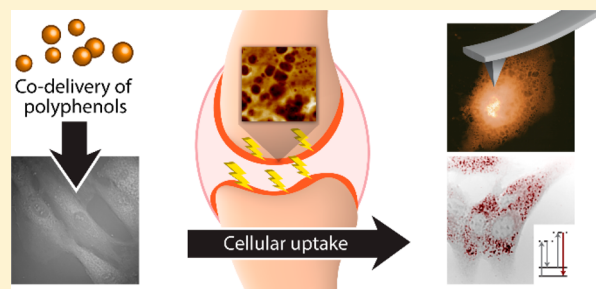
Because of a continuously growing understanding of origination and course of complex diseases on a molecular level, there is a high demand for sophisticated carrier systems allowing for intracellular delivery of active pharmaceutical ingredients (API) and thus treatment of such diseases on a subcellular level.

One example in this context is osteoarthritis, a multifactorial degenerative joint disease with a severe impact on life quality especially for the elderly population.[1] During the course of the disease, the chondrocytes within the cartilage tissue are inflamed, subsequently resulting in a breakdown of the connective tissue in the affected joint.[2−5] Despite this

knowledge, osteoarthritis is generally treated symptomatically using nonsteroidal, anti-inflammatory drugs limited to temporary effects without complete curing.[6,7] Recently, natural polyphenols gained considerable interest as therapeutic alternatives due to their anti-inflammatory, antioxidant, and chemo preventive potential.[3,8−10] It was shown that curcumin (diferuloylmethane) and resveratrol (*trans*-3,4′-trihydroxystilbene) have a protective effect on chondrocytes by modulating

the intracellular inflammation cascade.[6,11−13] Interestingly, this effect could even synergistically be increased by combining different polyphenols.[6,12] However, because of their low water solubility, the polyphenols were dissolved in organic solvents before application to cultivated chondrocytes.[6,11,14,15] Such organic solvents do not only artificially increase the solubility of the polyphenols but also increase the permeability of the chondrocytes. Thereby, the extent of intracellular uptake of the actives is artificially facilitated and increased which is not reflecting the *in vivo* situation in a human joint. To overcome these issues, we designed a delivery system for codelivery of resveratrol and curcumin based on self-assembling lipid-core nanocapsules (LNC) consisting of an oily core surrounded by a biocompatible and biodegradable shell of polycaprolactone (PCL).[16,17] These capsules provide protection and solubility enhancement for the lipophilic actives as well as a controlled release pattern.[18−20] Furthermore, a first study in a rat model of osteoarthritis showed promising results for LNC loaded with the polyphenols as a novel therapeutic approach.[21]

However, for in-depth understanding of such a novel approach for codelivery of two polyphenols, sophisticated analytics are required to elucidate cellular uptake and response. In terms of visualizing biological structures, research benefits from progress in microscopic techniques, especially in confocal laser scanning fluorescence microscopy for cell imaging. However, the technique requires biomarkers and these can cause misinterpretation of analytical results.[22,23] In addition to visualization, the analysis of cellular biomechanics upon drug application is important as inflammatory processes in osteoarthritic chondrocytes entail changes in their cell biomechanics and consequently their membrane structure.

In this study, we performed a multidisciplinary approach to bridge the aforementioned scientific gaps. We encapsulated resveratrol and curcumin in lipid-core nanocapsules and investigated their interactions with human primary chondrocytes. Further analysis focused on their therapeutic effects on the chondrocytes treated with a chemical NO-donor to induce apoptosis, thereby mimicking the conditions of diseased cells in osteoarthritic joints. To gain new insights, noninvasive and label-free coherent anti-Stokes Raman scattering (CARS) microscopy was used for visualization of interactions with chondrocytes and intracellular location of the capsules after uptake. Further, the cellular uptake process was elucidated by selective blocking of individual endocytosis pathways and subsequent CARS analysis. In addition, the therapeutic effect of the nanocapsules on chondrocytes was analyzed by a combination of bioassays and atomic force microscopy (AFM) to probe cellular nanobiomechanics and membrane structure as well as to investigate changes upon diseased state and therapeutic effects of the nanocapsules on human chondrocytes.

■ EXPERIMENTAL SECTION

Materials. Curcumin, poly(ε-caprolactone), sorbitan monostearate, 5-(*N*-ethyl-*N*-isopropyl) amiloride (ENIA), monensin sodium, chlorpromazine HCl, nystatin, sodium nitroprusside dehydrate (SNP), and methylthiazolyldiphenyl-tetrazolium bromide (MTT) as well as analytical solvents were purchased from Sigma-Aldrich. Grape seed oil was obtained from Delaware (Porto Alegre, Brazil). Resveratrol was supplied by Pharma Nostra (Anápolis, Brazil), and polysorbate 80 was acquired from Henrifarma (São Paulo, Brazil). All chemicals

and solvents were of pharmaceutical or HPLC grade and were used as received.

Preparation of Lipid-Core Nanocapsules. The protocol for LNC preparation was established by Jornada et al.[20] In brief, 27 mL of acetone including dissolved PCL (0.1 g), grape seed oil (165 μL) and sorbitan monostearate (0.0385 g) were injected into the aqueous phase (water 54 mL) containing polysorbate 80 (0.077g) under magnetic stirring at room temperature. Curcumin and/or resveratrol (5 or 2.5 mg) were part of the organic phase. Subsequently, acetone was eliminated under reduced pressure and the suspension was concentrated to a final volume of 10 mL. LNC containing 0.5 mg/mL of resveratrol (R-LNC) and curcumin (C-LNC) individually and in combination (Co-LNC) as well as polyphenol free nanocapsules were prepared. To investigate a possible dose dependent effect, LNC with 0.25 mg/mL of curcumin and resveratrol were fabricated additionally. For cell culture experiments a 50-fold dilution of LNC suspensions was used.

Characterization of Lipid-Core Nanocapsules. Physicochemical characteristics were acquired by photon correlation spectroscopy at a scattering angle of 173 °C for hydrodynamic size and polydispersity index (PdI) measurements and coupled with laser Doppler velocimetry to determine the zeta potential (Zetasizer Nano ZSP/SP, Malvern instruments, Malvern, U.K.). LNC suspensions were diluted in Milli-Q water (1/50) prior to measurements. The pH-value was directly determined from the LNC suspension using a calibrated potentiometer (VB-10, Denver Instrument Company, Colorado). Morphological characteristics were visualized by transmission electron microscopy (TEM) (JEM 2010, Tokyo, Japan). LNC suspensions, diluted in ultrapure water (200-fold) were placed on a specimen grid and counterstained with phosphotungstic acid hydrate (1% w/v). The microscope was operated at 200 kV. The *in vitro* release of resveratrol and curcumin from LNC was carried out by the dialysis bag method according to Coradini et al.[24] with minor modifications. A volume of 0.8 mL of the samples (Co-LNC, R-LNC, and C-LNC) were placed into a dialysis bag with a 10 kDa molecular weight cutoff and suspended into 80 mL of release medium (water/Tween 80/ethanol (80:2:20 v/v)). The samples ($n = 3$) were maintained at 37 °C under gentle agitation. At predetermined time intervals, 1 mL of release medium was withdrawn and replaced with fresh medium. The samples were diluted with mobile phase, filtered through a 0.45 μm membrane, and analyzed by the previously described HPLC method.[24]

Cell Culture Experiments. Human primary chondrocytes were purchased from PromoCell (Heidelberg, Germany) and cultured in chondrocyte growth medium (PromoCell) which was supplemented with 10% (v/v) fetal calf serum in an atmosphere of 5% CO_2 at 37 °C. During routinely performed subcultivation cells were seeded at a density of 20 000 cells/cm². Passages 9−11 were used for experiments.

CARS Microscopy. Chondrocytes were cultured in imaging dishes with a cover class insert in tissue culture quality. Preincubation with uptake inhibitors (5 μg/mL chlorpromazine, monensin, nystatin, ENIA) was done for 1 h prior to adding polyphenol-loaded LNC. To investigate energy dependent uptake, cells were moved to the refrigerator at 4 °C for LNC incubation. After 7 h in total the medium was replaced and dishes were moved onto the stage of the custom built CARS microscope, which is described in detail elsewhere.[25] The picosecond pulsed laser, which is coupled to the setup,

Table 1. Physicochemical Characteristics of Lipid-Core Nanocapsules in Aqueous Suspension and after 24 h Incubation in Cell Culture Medium (Mean Value ± SD, n = 3)

	in aqueous suspension			after 24 h in cell culture medium		
formulation	size (nm)	PdI	zeta potential (mV)	size (nm)	PdI	zeta potential (mV)
unloaded LNC	201.90 ± 1.95	0.077 ± 0.004	−22.43 ± 0.60	222.27 ± 1.67	0.159 ± 0.025	−4.40 ± 0.85
R-LNC	211.73 ± 1.65	0.093 ± 0.028	−21.73 ± 0.35	217.10 ± 1.65	0.140 ± 0.008	−5.73 ± 1.13
C-LNC	205.70 ± 1.04	0.077 ± 0.030	−22.17 ± 0.23	218.93 ± 1.81	0.168 ± 0.020	−4.81 ± 0.94
Co-LNC (1 mg/mL)	199.73 ± 0.93	0.115 ± 0.017	−20.97 ± 0.55	204.27 ± 0.67	0.154 ± 0.016	−3.56 ± 0.21
Co-LNC (0.5 mg/mL)	201.67 ± 1.80	0.067 ± 0.008	−22.50 ± 0.36	208.53 ± 2.82	0.143 ± 0.001	−4.49 ± 0.73

operated at a fundamental wavelength of 1032 nm (aeroPULSE-10, NKT Photonics, Birkerød, Denmark). An Olympus 60× water immersion objective was used to record the images.

Nitric Oxide Release. Chondrocytes were seeded in 96 well plates (10 000 cell per well, p10/11). Incubation times for LNC and 2 mM SNP (297.95 g/mol; 11.88 mg in 20 mL of medium) were 24 h. Cells were preincubated with LNC before exchanging for SNP solution. The Griess Reagent System (Promega Corporation, Madison, WI) was used according to provided instructions. For each assay a nitrite standard reference curve (0.1 M−0 M) was prepared in triplicate. The absorption of the formed purple colored azo compound was measured at 535 nm (Infinite M200Pro, Tecan GmbH, Crailsheim, Germany). Statistical analysis was performed using the student's t-test ($p < 0.05$).

Cell Viability Testing. Cell viability was investigated by the MTT assay (n = 8). Cells cultured in 96 well plates (10 000 cells/well) were washed with HBSS buffer prior to incubation with SNP for 24 h at 37 °C. As a positive control, 1% Triton X in medium was used. Cells were washed with HBSS and 100 μL of medium with 10% MTT reagent was added to each well. After 4 h of incubation on the shaker at 37 °C, the medium was exchanged for DMSO. After 30 min, the absorption of the formed formazan was measured at 550 nm (duration 5 s; amplitude 3 nm; Infinite M200Pro).

Atomic Force Microscopy. Chondrocytes were cultured in Petri dishes (10 000 cells/dish) with a growth area of 8.7 cm². The incubation time for Co-LNC and 2 mM SNP was 24 h each, where SNP was only applied after removing the medium containing nanocapsules. Subsequently, cells were fixed in 3% formaldehyde and air-dried just before AFM investigations. AFM images were recorded in air on a Dimension Fastscan Bio (Bruker-Nano, Santa Barbara, CA) operated in a dynamic force interaction control mode (Peak Force QNM) with Nanoscope 9 software. Silicon nitride tips were used (spring constants of 0.06 N/m, SNL-D tips from Bruker-Nano) as cantilevers with loading forces of approximately 1 nN. The lateral resolution of the depicted (50 μm)² AFM images is 48.8 nm/pixel. In the case of the (5 μm)² scans, the lateral resolution is 9.8 nm/pixel. Cross sectioning and bearing analyses of the images were carried out using Nanoscope Analysis software.

■ RESULTS AND DISCUSSION

The first step of this study involved a physicochemical and morphological analysis of the lipid-core nanocapsules loaded with the two polyphenols as well as their drug release kinetics. Jornada et al.[20] already proved that the granulometry profile of such lipid-core nanocapsules fabricated by interfacial deposition of PCL correlates with the concentration of raw materials in the aqueous and in the organic phase, respectively. Lipid-core nanocapsules were either loaded with curcumin or with

resveratrol (C-LNC, R-LNC, 0.5 mg polyphenol/mL) as well as with both polyphenols in combination (Co-LNC, 0.5 mg of each polyphenol/mL). For direct comparison between the effect of curcumin and resveratrol and their combination in terms of dose dependency and synergistic effects, an additional Co-LNC batch containing a total polyphenol dose of 0.5 mg/mL was included in the experiments. These Co-LNC (0.25 mg of each polyphenol/mL), which are introduced here for the first time, have a hydrodynamic diameter of 201.67 nm ±1.80 nm with a low size distribution (PdI 0.067 ± 0.008), a zeta potential of −22.50 mV ± 0.36 mV, and a pH value of 6.18 ± 0.21 in aqueous suspension. These physicochemical parameters are in good agreement with published data of C-LNC, R-LNC, and Co-LNC (0.5 mg/mL each), which have been investigated during the optimization of the LNC formulation for the encapsulation of the poorly water-soluble polyphenols.[24]

As hydrodynamic diameter, size distribution and zeta potential are important for evaluating the colloidal stability of LNC under cell culture conditions, these physicochemical characterization data for all generated nanocapsules in aqueous suspension are summarized in Table 1. As the comparison of unloaded capsules and capsules loaded with the different polyphenols proves, the fabrication process is well controlled and generates highly reproducible and physically stable nanocapsules. Drug loadings for lipid-core nanocapsules encapsulating resveratrol and/or curcumin are close to the theoretical value (R-LNC 0.49 mg/mL ± 0.01 mg/mL; C-LNC 0.49 mg/mL ± 0.02 mg/mL; Co-LNC 0.50 mg/mL ± 0.01 mg/mL (resveratrol); and 0.50 mg/mL ± 0.01 mg/mL (curcumin) as already published.[21,24,26] Consequently, the encapsulation efficiency is almost 100% for these formulations (R-LNC 98.00%; C-LNC 97.33%; Co-LNC 100.00% (resveratrol) and 99.33% (curcumin)). For this study, the physical stability of the lipid-core nanocapsules in cell culture medium is important to account for potential interactions with biomolecules in cell culture medium simulating the situation in the human body. The results of the physicochemical characterization of LNC after 24 h incubation in the medium at 37 °C are summarized in Table 1. All different LNC formulations are sized around 210 nm maintaining their narrow size range (PdI < 0.17) and a negative zeta potential. Low standard deviations suggest a homogeneous fraction of LNC despite different loadings. In comparison to LNC in aqueous suspension, the zeta potential decreases. The high values in aqueous suspension are potentially based on steric hindrances due to the presence of polysorbate 80 forming a micellar structure around the capsules.[27] In the presence of cell culture medium containing fetal calf serum among other nutritional supplements, this steric hindrance is most likely decreasing resulting in lower zeta potential values. Nevertheless, PdI values and standard deviations for investigated physicochemical characteristics remain as low as values obtained from LNC in aqueous

suspension. Thus, lipid-core nanocapsules retain their physicochemical characteristics in biorelevant media without agglomeration tendency which is frequently found for other nanocarriers.[28]

An expected round shape of the nanocapsules is confirmed by transmission electron microscopy images (Figure 1).
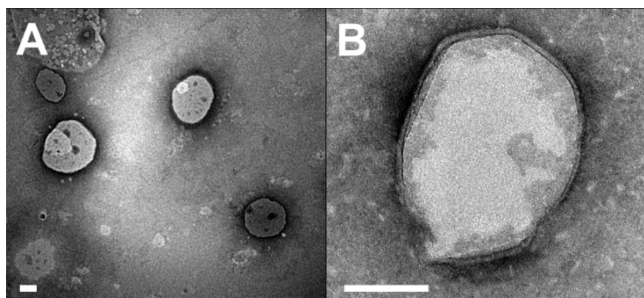
Figure 1. Representative transmission electron microscopy images showing LNC at a low magnification (10 000-fold) (A) and a close-up view showing the PCL wall (50 000-fold) (B). Scale bars denote 100 nm.

Additionally, the hydrodynamic size determined by photon correlation spectroscopy is in good agreement with the mean particle size observed during TEM analysis. The PCL wall of the nanocapsules surrounding the lipid core is homogeneous and has an estimated thickness of 8 nm.

Further, the release kinetics of the polyphenols from the nanocapsules were analyzed. The release of resveratrol (solid circle symbol) shows a steep slope which turns into a plateau phase after about 24 h, whereas curcumin (open circle symbol) release is much slower resulting in a continuous slope as depicted in Figure 2. Interestingly, neither coencapsulation of resveratrol and curcumin in the same capsules (dotted line versus straight line), nor the overall loading of the nanocapsules (0.5 mg/mL versus 1 mg/mL) does significantly change these kinetics.[24] However, a relationship between polyphenol solubility in grape seed oil, the main component of the capsule
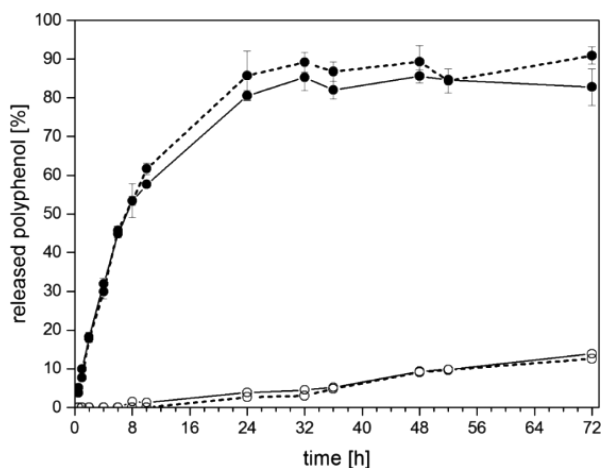
Figure 2. Drug release profiles of curcumin (○) and resveratrol (●) from lipid-core nanocapsules. Straight lines represent the capsules with one polyphenol, whereas dotted lines show the capsules loaded with both polyphenols (mean value ± SD, $n = 3$). For clarity reasons standard deviations for curcumin release which were ≤±2.64% are not shown.

core, and their different release kinetics was recently indicated. The solubility of resveratrol in grape seed oil was found to be 90 μg/mL and the solubility for curcumin in grape seed oil was determined as 475 μg/mL.[26] These solubility findings coincide well with the respective drug release, as a lower resveratrol solubility goes along with a faster release from the lipid-core nanocapsule, whereas the opposite is found for curcumin. The combination of synergistic actives like resveratrol and curcumin with different release kinetics bears a great potential for one single therapeutic system providing a fast initial therapeutic onset (resveratrol) in combination with prolonged treatment (curcumin) in one single application system.

However, physicochemical characterization of the polyphenol-loaded capsules as well as their *in vitro* release kinetics do not provide any information about the absorption into cells or the interplay of the two drugs. Osteoarthritis represents a potential therapeutic target for curcumin and resveratrol. The human joint as an application site for osteoarthritis treatment comprises a complex assembly of articular cartilage with chondrocytes as the predominant cell type. During the course of osteoarthritis, chondrocytes are severely inflamed, finally resulting into apoptosis and cartilage degeneration. It has already successfully been shown that resveratrol and curcumin have a positive effect on inflamed chondrocytes.[6,11,14,15] By encapsulating curcumin and resveratrol in lipid-core nanocapsules, we can improve their solubility circumventing the use of toxic organic solvents and at the same time avoiding precipitation. Thus, LNC facilitate the application of a higher dose delivery combined with a controlled drug release over longer therapy intervals. Further, the protective effect of nanocapsules on the polyphenols is highly beneficial.[24] In a first study, the therapeutic effect of LNC on complete Freund's adjuvant-induced arthritis in rats was tested.[21] Results were very promising especially for the formulation containing both polyphenols. Nevertheless, by using intraperitoneal injection, the administration site is far from the therapeutic target in the hind paw of the rat. Further, no experimental data were generated elucidating how the polyphenols reach the inflamed joint and their local uptake mechanism. For these investigations sophisticated analytics are necessary combining biological assays with high-end visualization techniques. In this context, we focus on cellular delivery of LNC using human chondrocytes to investigate the interplay of carrier, polyphenols, and cellular response by a multifactorial analytical approach.

The postulated pharmacological target for polyphenols in order to treat osteoarthritis is the intracellular inflammation cascade in which these substances are supposed to intervene.[6,11−13] Therefore, investigating the uptake of LNC into chondrocytes is of high interest including the potential to gain a deeper insight into their specific uptake mechanism.

For this purpose, we utilized coherent anti-Stokes Raman scattering (CARS) microscopy. This analytical method facilitates instantaneous visualization of the sample by solely detecting light scattering from an excited endogenous molecular structure The protein band at 2928 cm^{-1} is representative for the cell body. It was chosen to investigate cellular engulfment of LNC. The lipid core of the nanocapsules is the dominant structure of the carrier with the best scattering properties, thus the band for lipids located at 2845 cm^{-1} was set for LNC detection. The signal at both bands is accompanied by a nonresonant background that reveals the surrounding structure. Although cells naturally contain lipids themselves,

the local density of grape seed oil in the core provides a sufficient contrast for chemically selective imaging. In Figure 3,
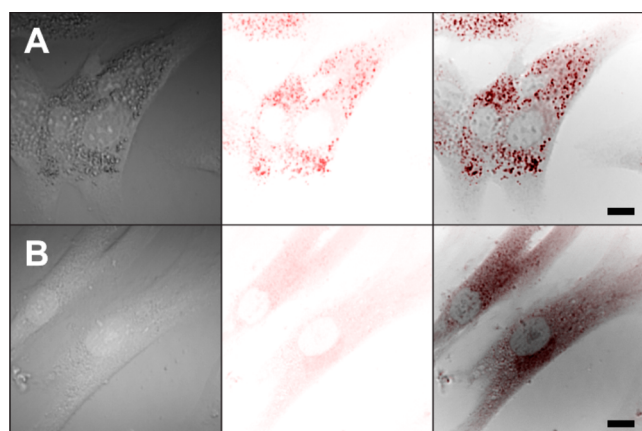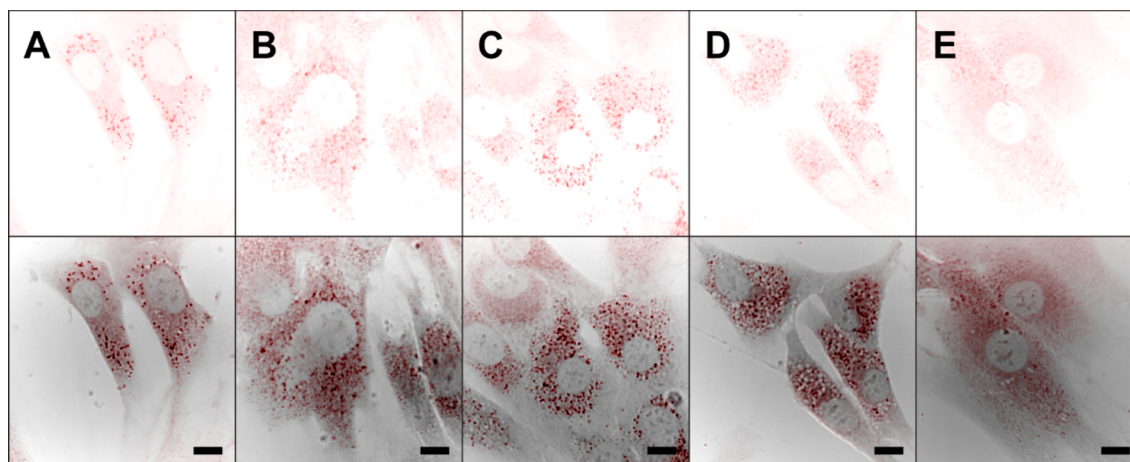

Figure 3. Coherent anti-Stokes Raman scattering microscopy images of chondrocytes engulfing lipid-core nanocapsules (A) and negative control chondrocytes (B). Left panels depict images generated by exciting the protein band. Center panels show false color background-free images of lipid location. Right panels show the overlay of left and center panels. Scale bars denote 10 μm.

the left panels depict plain cell bodies visualized by recording the protein band excitation, whereas the center panels were created by probing the lipid vibrations at 2548 cm^{-1} and using the common part of both images to remove the nonresonant background. For improved visualization and a clear differentiation in an overlap image (right panels), a MatLab algorithm was employed to create false color image based on the spectral data indication the background-free lipids in red color. The right panels depict an overlay of left and center panels.

Chondrocytes incubated with LNC are shown in Figure 3A. Cell bodies (left panel) show dark spots representing areas where molecular vibrations from proteins could not be sufficiently excited compared to the other cell parts. However, when comparing these dark spots with the false color lipid image (center panel), they colocalize with the prominent red spots. In these positions, the nanocapsules are located and their

lipid signal exceeds the intensity of the protein signal. Thus, in the presence of LNC, scattering of the proteins is barely detectable. The overlay image (right panel) underlies this spectroscopic signal contrast. A very light red hue is visible almost across the entire cell body. This observation is a logic consequence of the omnipresence of intracellular lipids especially in the cell walls. This hue is also present in the negative control chondrocytes visualized in Figure 3B. Nevertheless, the density of the grape seed oil in the nanocapsule core triggers an increased signal and its intensity is converted into a more intense color in the image, making the detection of LNC feasible even among other cellular lipids. Different incubation times were tested (6, 10, 24, and 72 h) to determine the maximum uptake. However, no obvious differences were detected, neither based on the duration of the incubation interval nor based on the different nanocapsule formulations (data not shown). Thus, all images presented here involve an exposure of chondrocytes to Co-LNC (1 mg/mL) for 6 h, as the major focus of the study is on the codelivery of both polyphenols.

There are different ways for a nanocarrier to enter a cell, mainly involving phagocytosis and nonphagocytic pathways.[17,29,30] Only a few specialized cells including macrophages and dendritic cells are able to perform phagocytosis, whereas nonphagocytic pathways occur ubiquitously.[30,31] These are categorized as micropinocytosis, clathrin-mediated endocytosis, caveolae-mediated endocytosis, and clathrin- as well as caveolae-independent endocytosis.[17,30] As chondrocytes do not belong to the group of specialized cells, most likely they do not engulf lipid-core nanocapsules by phagocytosis. Therefore, different uptake inhibitors were chosen based on the endocytic pathways for a more detailed investigation of the uptake mechanism of LNC into chondrocytes. Monensin was chosen to block clathrin- and caveolae-independent endocytosis.[32] In addition, chlorpromazine and nystatin were used to investigate if LNC uptake was driven by clathrin-mediated or caveolin-mediated endocytosis, respectively.[22,33] To examine micropinocytosis, amiloride (ENIA) was taken.[33] Chondrocytes were incubated with the respective inhibitors for 1 h before cells were exposed to LNC. CARS images were recorded to visualize potential uptake. Figure 4 depicts the CARS images with each row A–D showing experiments with another uptake


Figure 4. Coherent anti-Stokes Raman scattering microscopy images of chondrocytes exposed to lipid-core nanocapsules after preincubation with monensin (A), chlorpromazine (B), nystatin (C), ENIA (D), or at 4 °C (E). Upper panels depict CARS images generated by exciting lipid molecules. Lower panels show the overlay of cell body image and left panel. Scale bars denote 10 μm.

inhibitor. To discover possible effects of the inhibitors, the images were taken at fixed excitation intensities, scaled to the same size and are displayed at the same intensity scale. For all inhibitors, the upper panel depicts background-free CARS images acquired using the lipid frequency. Images in the lower panel show the overlay image of recorded lipid and protein band (Images after exciting the protein band are not depicted individually). There are no obvious differences in the uptake behavior of chondrocytes under the influence of the different inhibitors. All cells show a typical cell morphology, and LNC are visible in the cell body. LNC are located in the cytosol but could not be found in the nucleus. All images are comparable to the positive control but not to the negative control (Figure 3B). Therefore, monensin (Figure 4A), chlorpromazine (Figure 4B), nystatin (Figure 4C), and ENIA (Figure 4D), which are known to block nonendocytic pathways, do not hinder nanocasule engulfment by chondrocytes. Even switching to a higher concentration than 5 μg/mL did not lead to an uptake inhibition. Contrarily, apart from no effect for nystatin and monensin, higher concentrations had direct toxic effects on the cells (chlorpromazine, ENIA) preventing further examination (data not shown). Cytochalasin D which blocks macro-pincytosis and phagocytosis also had a toxic effect on chondrocytes even in lower contentrations. Because of morphological changes visible by light microscopy, this inhibitor was excluded from the studies. However, if cells were provided with fresh medium, they recovered which is in accordance with literature.[33] Phagocytosis is unlikely to be the engulfment mechanism due to the cell type, and the investigation of micropinocytosis was performed with amiloride. In order to examine if cellular uptake was driven by physical proximity of LNC and cell membrane, chondrocytes exposed to LNC were kept at 4 °C for the entire incubation period prior to CARS microscopy analysis to minimize energy-dependent processes like endocytosis.[22] The recorded images are depicted in Figure 4E in the same panel structure. Unlike images from inhibitor studies, CARS images in Figure 4E look similar to images of the negative control chondrocytes (Figure 3B). In both cases, the lipid-derived images consist of a red hue lacking deeply colored areas. Consequently, the local accumulation of lipid molecules represented by LNC are missing. Therefore, only lipids originating from the cell are detected and converted into images with a colored hue. The overlay image in the bottom panel visualizes the localization of the red hue over most parts of the cell body.

Thus, the uptake of LNC by human chondrocytes is most likely driven by the physical proximity of nanocapsules and cell membrane. No evidence was found that an inhibitor successfully blocked an endocytic uptake route.

As a next experimental step, the pharmacological effect of the nanocapsules is analyzed. For this a suitable readout is required. In this context, nitric oxide (NO) is a stimulus to cause apoptosis in chondrocytes and consequently progression of osteoarthritis, which has been found in high levels in osteoarthritic cartilage.[34] Sodium nitroprusside (SNP) is a NO generator which can be added to cell culture medium to investigate NO induced apoptosis mechanisms.[35−37] The increase of cellular reactive oxygen species (ROS), which are involved in many physiological cell functions, is triggered by exogenous nitrite oxide.[37,38] However, ROS becomes cytotoxic once its level exceeds a threshold marked by the cell's antioxidant ability.[37,39] To determine this threshold, we performed an MTT assay after incubating chondrocytes with

SNP at different concentrations for 24 h. After 24 h, only 19.52% ± 0.04% ($n = 8$) of the cells were viable when exposed to 2 mM SNP, while the viability remained high for incubation experiments with 1.5 mM and 1 mM SNP (93.05% ± 0.04% and 108.33% ± 0.04%, respectively; $n = 8$). Thus, 2 mM SNP was used in the subsequent experiments to investigate if polyphenol loaded LNC have a protective effect against SNP induced oxidative stress. The results are depicted in Figure 5.
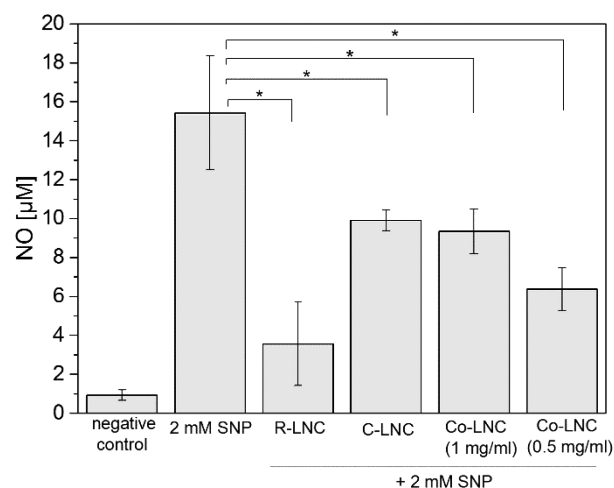
Figure 5. Nitric oxide (NO) levels expressed by chondrocytes under the influence of sodium nitroprusside (SNP) and a preincubation with different lipid-core nanocapsules ($n \geq 3$). Calculations are based on a standard calibration curve ($n = 3$). Statistical significance ($p < 0.05$) is indicated by *.

Chondrocytes express nitrite oxide (NO), as the molecule is a physiological messenger. Under the influence of 2 mM SNP, the NO level significantly increases. Similar to cell viability measurements, the level of NO depends on the SNP concentration. Incubation with 1 mM SNP resulted in 8.8 μM ± 1.5 μM of nitric oxide, whereas application of 1.5 mM SNP resulted in a readout of 11.2 μM ± 0.6 μM NO ($n = 10$). After preincubation with LNC, the amount of expressed NO significantly decreases ($p < 0.05$). The lowest value was found for R-LNC followed by Co-LNC (0.5 mg/mL), Co-LNC (1 mg/mL), and C-LNC. The contrary findings for R-LNC and C-LNC are very plausible as they correlate with the drug release profiles (Figure 2). Resveratrol shows the fastest release and is thus immediately available to scavenge ROS, consequently protecting chondrocytes, which is represented by the expression of low nitric oxide values (Figure 5, R-LNC). In contrast, a highly protective effect of curcumin is hardly expectable as only 3.9% ± 0.3% of the polyphenol are released after 24 h. Consequently, the expression of NO levels is rather high (Figure 5, C-LNC). Interestingly, the effect of coencapsulated polyphenols is in-between the results for R-LNC and C-LNC, respectively. Although the release profiles of the individual polyphenols from the combined formulation are coinciding with their counterparts R-LNC and C-LNC, resveratrol does not perform accordingly as the NO values at least for Co-LNC containing 0.5 mg/mL of resveratrol would be expected to be similar to R-LNC results. A study by Liang et al.[40] showed that resveratrol applied in solution prevented the SNP induced production of reactive oxygen species in rabbit chondrocytes as the polyphenol scavenged ROS. The authors proposed a signaling pathway which is invaded by resveratrol
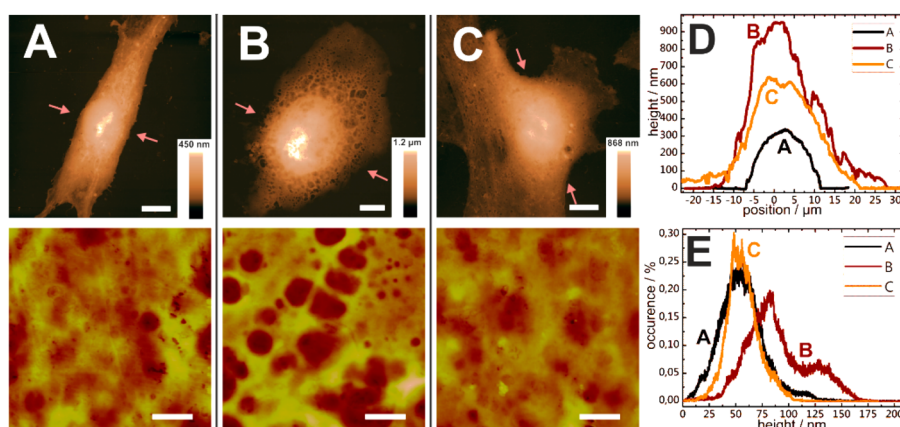
Figure 6. Atomic force microscopy analysis of chondrocytes as control (A), exposed to 2 mM SNP (B), and preincubation with Co-LNC prior to SNP exposure (C). Panels in the upper row show the entire cell bodies acquired in tapping mode (scale bars are 10 μm). Panels in the lower row show a close up of the cell surfaces with a z-scale of 200 nm (scale bars are 1 μm). Panel D shows cross sections of all cells through their highest point (indicated by the small arrows in parts A−C, upper panels). Panel E displays the results of bearing analysis from all closeup scans.

before ROS reaches the mitochondria. Curcumin was not included in this study. However, multiple studies employing curcumin and/or resveratrol are published where IL-1β was used to trigger inflammation in chondrocytes.[6,13,15,41,42]

Csaki et al.[6] studied synergistic effects of dissolved curcumin and resveratrol on chondrocytes upon exposure to IL-1β. The authors proposed that both polyphenols intervene in the same intracellular reaction cascade; however, curcumin interferes earlier than resveratrol. Implying a similar situation for the SNP induced mechanism, our findings lead to the following conclusions: Delivery of polyphenols by LNC and different release profiles seem to influence the protective effects of the two polyphenols and hinder a synergistic effect when codelivered in this case. Thus, the detected NO levels for nanocapsules comprising both polyphenols are higher than results for R-LNC but lower than results for C-LNC. Furthermore, the polyphenol loading of Co-LNC seems to have an impact as well. Detected NO values for Co-LNC encapsulating 0.5 mg/mL are lower than for an encapsulated polyphenol concentration of 1 mg/mL. Less curcumin is available in Co-LNC (0.5 mg/mL) to interfere with resveratrol effects, strengthening the protective effect resveratrol against SNP induced apoptotic effects by nitric oxide. While physicochemical characteristics did not show any influence on uptake behavior between capsules carrying various polyphenol loads as determined by CARS microscopy analysis, we gain a different insight from the NO-assay. Thus, this analysis is an illustrative example for the importance of research approaches using different complementary techniques to gain a "big picture" rather than relying on one single analysis. Even though the NO-assay provides interesting insight into the mechanism and interaction of the two polyphenols, the results are not suited for evaluating the overall "therapeutic effect" of the LNC codelivering the two polyphenols as the comparison with other analytical techniques shows. Further, a generally neglected factor is posed by changes of cell membrane and cytoskeleton of the cells upon induced inflammation and application of drugs.

In this context, AFM has lately been employed to detect physical differences between healthy and diseased cells, as cellular ultrastructures tend to alter in diseased or cancerous cells.[43−45] The high spatial resolution of this technique enables the investigation of cell membrane properties.[46] AFM provides

an attractive addition to conventional visualization and molecular biological assays in order to gain further information on cellular surface topography. Here, we use AFM to study the apoptotic effect of SNP and the preventive abilities of Co-LNC on cell morphology and membrane nanostructure of human chondrocytes.

AFM analysis was performed with chondrocytes without any treatment (control), after treatment with 2 mM SNP as well as after preincubation with Co-LNC prior to SNP exposure. Representative AFM images of the entire cell body as well as close-ups of the cell surface are displayed in Figure 6A−C. The control chondrocyte shows an elongated cell body with a rather homogeneous height forming lamellopodia in order to get into contact with other cells (Figure 6A). In contrast, the chondrocyte treated with 2 mM SNP presents a rather round, contracted shape with a structured surface, which is generally expected upon cell exposure with toxic substances and apoptosis (Figure 6B). These results are corroborated by results from MTT analysis showing that cell viability severely drops to 19.52% ± 0.04 after incubation with 2 mM SNP. A cell which was pretreated with Co-LNC prior to SNP exposure is shown in Figure 6C. Interestingly, in comparison to Figure 6A,B, the cell rather shows similarity to the untreated cell and defects due to SNP exposure (as seen in Figure 6B) are neglectable. Besides morphology analysis, height profiles of the cells were acquired. For all chondrocytes, the nucleus represents the highest area of the cell body, as displayed in Figure 6D. The differences in morphology revealed in Figures 6A−C are reflected in the height profiles. The control chondrocyte has a height of about 300 nm, whereas the cell treated with SNP is more than 3 times higher. When pretreated with Co-LNC prior to SNP, the cell height only increases to approximately 600 nm. Thus, the effect of SNP on cell height and morphology is significantly attenuated by polyphenol loaded LNC. To study changes in the cell membrane in more detail, close-up AFM images were recorded (Figure 6A−C, lower panel). Again, the images taken from control chondrocytes and cells pretreated with LNC depict a similar membrane structure. On the contrary, the cell membrane of SNP exposed chondrocytes exposes dents and bumps. Again, AFM analysis shows the protective effect of polyphenol-loaded LNC against SNP exposure. Nanocapsules delivering resveratrol and curcumin into the cell are likely to have a protective impact on chondrocytes against SNP. To

quantify the differences in surface morphology, a subsequent bearing analysis was performed (Figure 6E). The control chondrocyte and the Co-LNC pretreated cell show very similar height distributions with a maximum at approximately 50 nm. The SNP treated cell without protective pretreatment shows a different height distribution with two maxima at 75 and 140 nm, respectively. This reflects the visualized surface pattern well, as the two maxima can directly be correlated to the pitted surface structure.

Overall, the results of the AFM study are in good agreement with confocal fluorescence microscopy investigations by Liang et al. showing a remodeling of the cell's cytoskeleton upon exposure to SNP.[40] F-actin filaments shortened, microtubule structures were disrupted and thus the cell shrunk, which is observable in the AFM image in Figure 6B. A preincubation with resveratrol prevented these extreme effects on the cell, which can be substantiated by our findings. In this context, AFM investigations expanded the insight into the interplay between cells and carrier by visualizing cellular reactions and the advantage of combining different analytical procedures to create a more comprehensive picture in spite of a snapshot becomes evident. Overall, the nanocapsules have a positive effect on cellular nanobiomechanics reflected in the cell membrane morphology preventing damage leading to cell death by an externally applied nitric oxide donor.

CONCLUSIONS

In summary, we have successfully combined biological assays with sophisticated nondestructive, label-free microscopic techniques (CARS and AFM) for the an all-encompassing investigation of the therapeutic effects of advanced nanocapsules loaded with two polyphenols against induced osteoarthritic states of human chondrocytes. CARS microscopy images depict a clear uptake of the well-characterized lipid-core nanocapsules into the cellular cytosol. However, no distinct endocytotic pathway could be determined and cellular uptake was found to be energy dependent. The extent of these effects was found to be determined by the drug release kinetics from the capsules as well as by their drug loadings. Findings from these assays were underlined by AFM studies visualizing a protective effect on cell morphology and membrane surface as a result of chondrocytes treatment with the polyphenol-loaded nanocapsules. Thus, besides presenting a sophisticated carrier system for joint application, these results highlight the necessity and potential of establishing combinatorial analytical approaches to elucidate cellular uptake, the interplay of codelivered drugs, and their therapeutic effect on the subcellular level to gain a "big picture" for in-depth understanding of novel therapeutic approaches.

AUTHOR INFORMATION

Corresponding Author
*E-mail: m.windbergs@mx.uni-saarland.de. Fax: +49 681 98806 1009.

Author Contributions
The manuscript was written through contributions of all authors. All authors have given approval to the final version of the manuscript.

Notes
The authors declare no competing financial interest.

REFERENCES
(1) van der Kraan, P. M.; van den Berg, W. B. *Ageing Res. Rev.* **2008**, 7, 106−113.
(2) Goldring, M. B. *Arthritis Rheum.* **2000**, 43, 1916−1926.
(3) Im, H. J.; Li, X.; Chen, D.; Yan, D.; Kim, J.; Ellman, M. B.; Stein, G. S.; Cole, B.; Kc, R.; Cs-Szabo, G.; van Wijnen, A. J. *J. Cell. Physiol.* **2012**, 227, 3488−3497.
(4) Malemud, C. J.; Islam, N.; Haqqi, T. M. *Cells Tissues Organs* **2003**, 174, 34−48.
(5) van der Kraan, P. M.; Buma, P.; van Kuppevelt, T.; van den Berg, W. B. *Osteoarthritis Cartilage* **2002**, 10, 631−637.
(6) Csaki, C.; Mobasheri, A.; Shakibaei, M. *Arthritis Res. Ther.* **2009**, 11, R165.
(7) Jin, H.; Liang, Q.; Chen, T.; Wang, X. *PLoS One* **2014**, 9, e91611.
(8) Wadsworth, T. L.; Koop, D. R. *Biochem. Pharmacol.* **1999**, 57, 941−949.
(9) Bisht, K.; Wagner, K. H.; Bulmer, A. C. *Toxicology* **2010**, 278, 88−100.
(10) Shen, C. L.; Smith, B. J.; Lo, D. F.; Chyu, M. C.; Dunn, D. M.; Chen, C. H.; Kwun, I. S. *J. Nutr. Biochem.* **2012**, 23, 1367−1377.
(11) Shakibaei, M.; Schulze-Tanzil, G.; John, T.; Mobasheri, A. *Ann. Anat.* **2005**, 187, 487−497.
(12) Shakibaei, M.; Mobasheri, A.; Buhrmann, C. *Genes Nutr.* **2011**, 6, 171−179.
(13) Csaki, C.; Keshishzadeh, N.; Fischer, K.; Shakibaei, M. *Biochem. Pharmacol.* **2008**, 75, 677−687.
(14) Shakibaei, M.; Csaki, C.; Nebrich, S.; Mobasheri, A. *Biochem. Pharmacol.* **2008**, 76, 1426−1439.
(15) Shakibaei, M.; John, T.; Schulze-Tanzil, G.; Lehmann, I.; Mobasheri, A. *Biochem. Pharmacol.* **2007**, 73, 1434−1445.
(16) Sinha, V. R.; Bansal, K.; Kaushik, R.; Kumria, R.; Trehan, A. *Int. J. Pharm.* **2004**, 278, 1−23.
(17) Hillaireau, H.; Couvreur, P. *Cell. Mol. Life Sci.* **2009**, 66, 2873−2896.
(18) Ourique, A. F.; Pohlmann, A. R.; Guterres, S. S.; Beck, R. C. *Int. J. Pharm.* **2008**, 352, 1−4.
(19) Fontana, M. C.; Coradini, K.; Guterres, S. S.; Pohlmann, A. R.; Beck, R. C. *J. Biomed. Nanotechnol.* **2009**, 5, 254−263.
(20) Jornada, D. S.; Fiel, L. A.; Bueno, K.; Gerent, J. F.; Petzhold, C. L.; Beck, R. C. R.; Guterres, S. S.; Pohlmann, A. R. *Soft Matter* **2012**, 8, 6646−6655.
(21) Coradini, K.; Friedrich, R. B.; Fonseca, F. N.; Vencato, M. S.; Andrade, D. F.; Oliveira, C. M.; Battistel, A. P.; Guterres, S. S.; da Rocha, M. I.; Pohlmann, A. R.; Beck, R. C. *Eur. J. Pharm. Sci.* **2015**, 78, 163−170.
(22) Herd, H.; Daum, N.; Jones, A. T.; Huwer, H.; Ghandehari, H.; Lehr, C. M. *ACS Nano* **2013**, 7, 1961−1973.
(23) Torchilin, V. P. *Adv. Drug Delivery Rev.* **2005**, 57, 95−109.
(24) Coradini, K.; Lima, F. O.; Oliveira, C. M.; Chaves, P. S.; Athayde, M. L.; Carvalho, L. M.; Beck, R. C. R. *Eur. J. Pharm. Biopharm.* **2014**, 88, 178−185.
(25) Garbacik, E. T.; Herek, J. L.; Otto, C.; Offerhaus, H. L. *J. Raman Spectrosc.* **2012**, 43, 651−655.
(26) Friedrich, R. B.; Kann, B.; Coradini, K.; Offerhaus, H. L.; Beck, R. C. R.; Windbergs, M. *Eur. J. Pharm. Sci.* **2015**, 78, 204−213.
(27) Sabuncu, A. C.; Kalluri, B. S.; Qian, S.; Stacey, M. W.; Beskok, A. *Colloids Surf., B* **2010**, 78, 36−43.
(28) Allouni, Z. E.; Cimpan, M. R.; Hol, P. J.; Skodvin, T.; Gjerdet, N. R. *Colloids Surf., B* **2009**, 68, 83−87.

(29) Conner, S. D.; Schmid, S. L. *Nature* **2003**, *422*, 37−44.

(30) Zaki, N. M.; Tirelli, N. *Expert Opin. Drug Delivery* **2010**, *7*, 895−913.

(31) Aderem, A.; Underhill, D. M. *Annu. Rev. Immunol.* **1999**, *17*, 593−623.

(32) Pohlmann, R.; Kruger, S.; Hasilik, A.; Von Figura, K. *Biochem. J.* **1984**, *217*, 649−658.

(33) Nakase, I.; Niwa, M.; Takeuchi, T.; Sonomura, K.; Kawabata, N.; Koike, Y.; Takehashi, M.; Tanaka, S.; Ueda, K.; Simpson, J. C.; Jones, A. T.; Sugiura, Y.; Futaki, S. *Mol. Ther.* **2004**, *10*, 1011−1022.

(34) Diaz-Gallego, L.; Prieto, J. G.; Coronel, P.; Gamazo, L. E.; Gimeno, M.; Alvarez, A. I. *J. Orthop. Res.* **2005**, *23*, 1370−1376.

(35) Blanco, F. J.; Ochs, R. L.; Schwarz, H.; Lotz, M. *Am. J. Pathol.* **1995**, *146*, 75−85.

(36) Tonomura, H.; Takahashi, K. A.; Mazda, O.; Arai, Y.; Inoue, A.; Terauchi, R.; Shin-Ya, M.; Kishida, T.; Imanishi, J.; Kubo, T. *Osteoarthritis Cartilage* **2006**, *14*, 545−553.

(37) Wu, G. J.; Chen, T. G.; Chang, H. C.; Chiu, W. T.; Chang, C. C.; Chen, R. M. *J. Cell. Biochem.* **2007**, *101*, 1520−1531.

(38) Lo, Y. Y.; Conquer, J. A.; Grinstein, S.; Cruz, T. F. *J. Cell. Biochem.* **1998**, *69*, 19−29.

(39) Stoop, R.; Buma, P.; van der Kraan, P. M.; Hollander, A. P.; Billinghurst, R. C.; Poole, A. R.; van den Berg, W. B. *Arthritis Rheum.* **2000**, *43*, 2121−2131.

(40) Liang, Q.; Wang, X.-p.; Chen, T.-s. *Apoptosis* **2014**, *19*, 1354−1363.

(41) Mathy-Hartert, M.; Jacquemond-Collet, I.; Priem, F.; Sanchez, C.; Lambert, C.; Henrotin, Y. *Inflammation Res.* **2009**, *58*, 899−908.

(42) Lei, M.; Wang, J.-g.; Xiao, D.-m.; Fan, M.; Wang, D.-p.; Xiong, J.-y.; Chen, Y.; Ding, Y.; Liu, S.-l. *Eur. J. Pharmacol.* **2012**, *674*, 73−79.

(43) Cross, S. E.; Jin, Y. S.; Tondre, J.; Wong, R.; Rao, J.; Gimzewski, J. K. *Nanotechnology* **2008**, *19*, 384003.

(44) Iyer, S.; Gaikwad, R. M.; Subba-Rao, V.; Woodworth, C. D.; Sokolov, I. *Nat. Nanotechnol.* **2009**, *4*, 389−393.

(45) Lee, G. Y.; Lim, C. T. *Trends Biotechnol.* **2007**, *25*, 111−118.

(46) Lesniewska, E.; Emmanuel Milhiet, P.; Giocondi, M.-C.; Le Grimellec, C. In *Methods in Cell Biology*, Bhanu, P. J., Hörber, J. K. H., Eds.; Academic Press: New York, 2002; pp 51−65.